

# Prediction of the sheet thickness effect on the formability of brass CuZn37 in single point incremental forming using Hooputra ductile damage model

Marwa K. Qate'a<sup>1\*</sup>, Adnan I. Mohammed<sup>1</sup>, Muhsin J. Jweg<sup>2</sup> 

<sup>1</sup> Production Engineering and Metallurgy Department, University of Technology, Al-Sena'ah Str., Karadah, 10066, Baghdad, Iraq

<sup>2</sup> AlFarahidi University, Baghdad, 00965, Iraq

\* Corresponding author's e-mail: [pme.20.67@grad.uotechnology.edu.iq](mailto:pme.20.67@grad.uotechnology.edu.iq)

## ABSTRACT

Single point incremental forming (SPIF) is a novel and practical approach for quickly prototyping and producing small batch sheet metal components. Predicting the impact of sheet thickness in the SPIF process is vital for assessing forming limits, understanding material behavior, optimizing tool design and path, and improving material utilization. It enables engineers to make informed decisions and optimize the process for enhanced formability and part quality. In this work, the numerical simulation of formability of the hyperbolic truncated pyramid with varying wall angles from 20° to 80° by the implementation of the Hooputra ductile damage (HDD) model in Abaqus/Explicit with the version of (CAE, 2017) has been conducted for brass of CuZn37 to study and predict the impact of the material's sheet thickness on its formability in SPIF process. In addition to that, the effect of sheet thickness on three other output responses: Von Mises stress, equivalent plastic strain, and contact pressure, have been examined. The results demonstrated the excellent success of the Hooputra ductile damage model in simulating the formability and capturing the fracture in the SPIF process with a total error ratio of approximately 1.91%. The results also showed that increasing sheet thickness from 0.4–1.4 mm increases formability, Von Mises stress, and contact pressure while leading to decreases and then increases the equivalent plastic strain.

**Keywords:** SPIF, Hooputra ductile damage model, brass CuZn37, numerical simulation, formability.

## INTRODUCTION

Incremental sheet forming (ISF) is a process for shaping sheet materials that can create complex geometries without requiring specialized dies. The process typically involves a hemispherical tool that follows the contours of the desired shape, gradually increasing in depth. Because it does not require forming dies, this method is well-suited for low- to medium-volume production. However, its adoption in the industry is hindered by several challenges, such as springback and poor surface finishes [1–3]. The SPIF process has gained greater prominence today, and according to its advantages over traditional forming methods, it is seen as more promising for meeting modern industry demands and trends [4, 5]. The

advantages of the ISF process include improved formability of sheet metal products [6] and meeting the needs of various industrial fields, including automotive industry, aerospace, and the biomedical applications [7–9]. In 2004, a research team at BMW in Germany, led by Hooputra, developed a comprehensive approach for predicting component failure using macroscopic strain and stress data. This method integrates different failure mechanisms, such as necking from local instabilities and both ductile and shears fractures. The failure criteria were specifically designed to account the effects of non-linear strain paths. The team experimentally determined the material damage parameters for 7076 aluminum alloy under both quasi-static and dynamic conditions, successfully predicting fractures in the components.

The Hooputra ductile damage criterion is a phenomenological model that predicts damage initiation through the nucleation, growth, and merging of voids [10] based on Kolmogorov's mathematical model [11] and assumes that the equivalent plastic strain at the initiation of damage is influenced by stress triaxiality and strain rate. Gatea et al. [12] introduced a modified Gurson-Tvergaard-Needleman (GTN) damage model that includes shear effects to predict ductile fracture in the SPIF process caused by void nucleation and coalescence. In comparison to the original GTN model used in SPIF, the results showed that the shear-modified version offered enhanced accuracy in predicting fractures under shear-loading conditions. Khan and Pradhan [13] performed and compared both experimental and numerical analyses on the formability of Aluminum 8011 by producing a conical frustum shape through the SPIF process. The tool path for the hemispherical tool tip was generated using a CATIA manufacturing simulation model. Response variables such as temperature, thickness reduction, strain, and machining time were analyzed. The experimental findings were in close agreement with the results from the numerical simulations. Sureshkumar and Ethiraj [14] carried out experimental studies and numerical simulations using the LS-DYNA explicit solver to identify the maximum wall angle that could be achieved at a specific depth without defects. Their findings revealed that major strain, minor strain, and thinning were more significant in areas below the major diameter of the truncated cone. More et al. [15] evaluated formability using the GTN model. The GTN parameters were optimized through response surface methodology (RSM). The findings were consistent with experimental results, and the GTN model predicted the forming depth satisfactorily. Campanella et al. [16] developed a numerical approach to derive an analytical expression for material formability in hot incremental forming processes. They employed the Johnson-Cook material model and validated it using experimental data obtained from the ARAMIS system. A strong correlation was found between the numerically computed PEEQ values and the sheet thinning. Zhang et al. [17] utilized an improved Continuum Damage Mechanics model to predict ductile damage in SPIF. This model is based on the von Mises yield criterion and incorporates non-linear mixed isotropic and kinematic hardening. The enhanced CDM model was integrated into the FE code Abaqus/

Explicit using the VUMAT user subroutine. The simulation results showed excellent correlation with experimental data.

Despite the significant progress in formability simulation in single point incremental forming, accurate fracture prediction still represents a challenge due to the complex states of stress and the gradual nature of deformation. Many traditional damage models, such as Gurson-Tvergaard-Needleman (GTN) and Johnson-Cook, have been widely used for this purpose, but they often fail to account for the combined impact of stress triaxiality and strain rate, which plays an important role in ductile fracture. The present work proposes a novel approach by applying the Hooputra Ductile Damage (HDD) model, based on stress triaxiality and fracture strain, to simulate the SPIF using ABAQUS/Explicit software. This model introduces a more accurate simulation of SPIF and predicts the onset of fracture through a set of process parameters, which provides a new criterion for damage in SPIF. The numerical simulation of formability of a hyperbolic truncated pyramid with varying wall angles from 20° to 80° by the implementation of this model as a fracture damage criterion has been performed for brass CuZn37 material to capture the fracture, and then used this model to predict the effect of sheet thickness of material on its formability. In addition, it examined the effect of sheet thickness on three other output responses: Von Mises stress, equivalent plastic strain, and contact pressure. The results of this work are expected to enhance process optimization and improve material selection and process efficiency in the industrial application of this process.

## MATERIAL AND EXPERIMENTAL WORK

Brass CuZn37 sheet material with a dimension of 150 × 150 × 0.8 mm has been executed in a SPIF process using PENNZOIL (SAE 5w-30) as a lubricant. A tensile specimen has been cut from the brass CuZn37 sheets at 90° (perpendicular) to the rolling direction according to the ASTM E8M standard to conduct the tensile test of this standard specimen that depicted in Figure 1. The Laryee Universal Testing Machine UTM (WDW-50), used for determining the mechanical properties of Brass CuZn37, meets the Class 0.5 standard according to ASTM E4, ISO75001, ensuring a force measurement accuracy of ± 0.5%

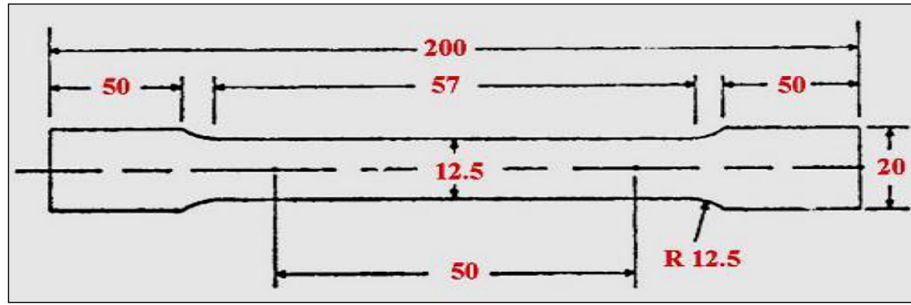


Figure 1. The E8/E8M ASTM tensile test specimen

as depicted in Figure 2; Table 1 illustrates the mechanical properties of CuZn37. The strength coefficient (K) and Strain hardening exponent (n) of the brass CuZn37 in the as-delivery conditions have been determined using the standard tensile test specimen and the true strain and true stress have been determined from the engineering strain and stress using the following Equations:

$$\epsilon_{true} = \ln(1 + \epsilon_{eng}) \quad (1)$$

$$\sigma_{true} = \sigma_{eng} \times (1 + \epsilon_{eng}) \quad (2)$$

where:  $\epsilon_{eng}$  is the engineering strain ( $\Delta L/L_0$ ), which is the change in length divided by the original length, and  $\sigma_{eng}$  is the engineering stress ( $F/A_0$ ), calculated as the force divided by the original cross-sectional area. To determine K and n, the following flow curve equation has been used:

$$\sigma_{true} = K \times \epsilon_{true}^n \quad (3)$$

By using the curve fitting method in Excel, K and n were measured approximately as  $K = 837$  and  $n = 0.44$  and the flow curve equation became as follows:

$$\sigma_{true} = 837 \times \epsilon_{true}^{0.44} \quad (4)$$

This brass alloy has been used to form a hyperbolic truncated pyramid with varying wall angles from (20–80°) according to the dimensions in Figure 3. Solidworks software designed the CAD model, and the (z level) tool path was

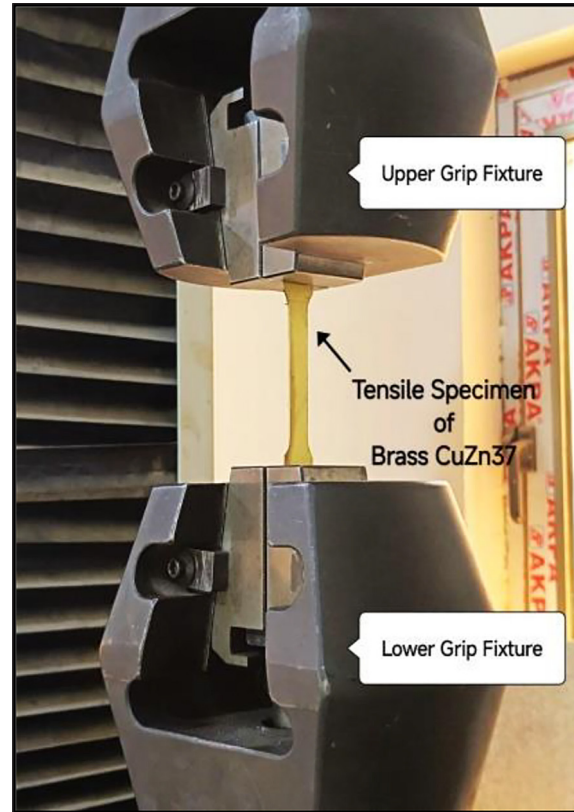


Figure 2. Tensile testing of Brass CuZn37

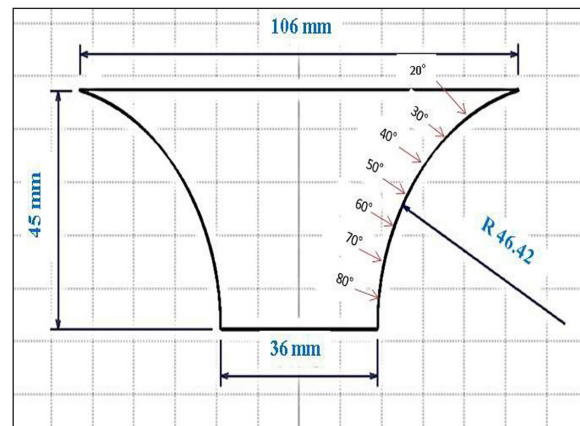


Figure 3. Dimensions of the hyperbolic truncated pyramid with varying wall angles

Table 1. Mechanical properties of brass CuZn37

| Mechanical property               | Value |
|-----------------------------------|-------|
| Offset yield stress (MPa)         | 254   |
| Tensile strength (MPa)            | 503   |
| Modulus of elasticity (GPa)       | 97    |
| Elongation %                      | 64    |
| Density (g/cm <sup>3</sup> ) [18] | 8.45  |
| Poisson's ratio [18]              | 0.34  |

generated by HSMWORKs software to form this product. Four experiments were performed using a three-axis CNC vertical milling machine C-tek model KM-80D, as depicted in Figure 4. The fracture depth has been measured directly from the CNC controller screen. When the fracture occurs, we turn off the CNC machine directly and then read the amount of the depth (displacement in the Z-axis). This fracture depth is considered a formability indicator of SPIF. Table 2 illustrates the input parameters of these experiments and the measuring output, and Figure 5 depicts the experimental specimens with the fracture zones.

### FINITE ELEMENT SIMULATION

ABAQUS/Explicit simulates the SPIF process; Abaqus software works depending on an algorithm built using the finite element method. Finite element analysis (FEA) is a method used in engineering and science to address specific problems, usually in an approximate way. It is mainly

applied to problems with no exact mathematical solution or cannot be represented in a precise mathematical form. FEA is a numerical approach rather than an analytical one [19]. In this work and to simulate the SPIF process, the sheet material (brass CuZn37) was modeled as a 3D deformable part with a solid shape and extrusion type as a base feature and with isotropic elastic and plastic-yielding material properties. In contrast, the forming tool with a diameter of 10 mm was modeled as 3D analytical rigid part with an extruded shell as the base feature. A surface-to-surface contact (Explicit) interaction type was created between the forming tool and the blank sheet with a coefficient of friction of 0.1. Moreover, three types of boundary conditions have been created as follows: the first type of boundary condition is the (Symmetry/Antisymmetry/Encastre) type, which is used to clamp the blank sheet periphery and prevent it from bending; the second type is the (Displacement/Rotation) type which is used to insert the time and amplitudes to the forming tool in (x, y, z) directions and giving it the motion,

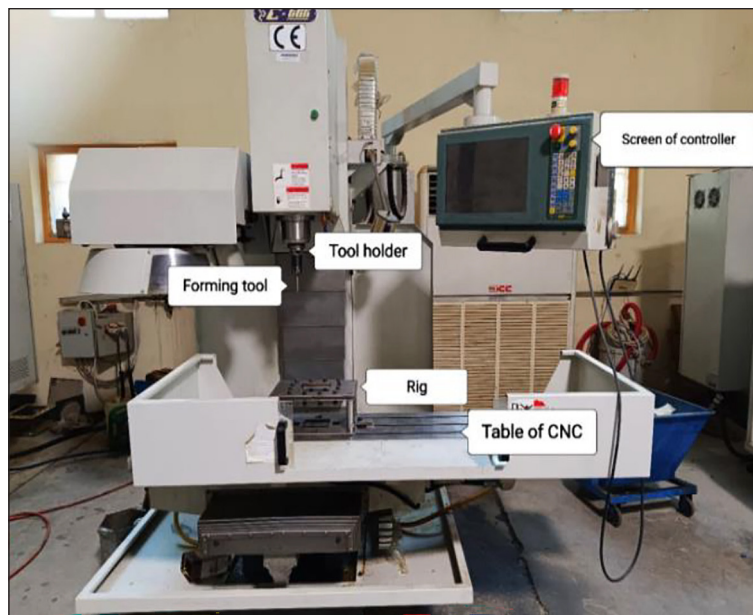


Figure 4. CNC milling machine (C-tek model KM-80D) with the SPIF fixture

Table 2. Input parameters of SPIF experiments with the measured outputs

| Exp. No. | Input parameters |                    |                           |                    |                |                      | Output                 |
|----------|------------------|--------------------|---------------------------|--------------------|----------------|----------------------|------------------------|
|          | Type of material | Feed rate (mm/min) | Tool rotation speed (rpm) | Tool diameter (mm) | Step size (mm) | Sheet thickness (mm) | Depth of fracture (mm) |
| 1        | CuZn37           | 800                | 1500                      | 10                 | 0.7            | 0.8                  | 34.4                   |
| 2        | CuZn37           | 1200               | 700                       | 10                 | 0.7            | 0.8                  | 30.8                   |
| 3        | CuZn37           | 1200               | 1500                      | 10                 | 0.3            | 0.8                  | 25.2                   |
| 4        | CuZn37           | 1200               | 1500                      | 10                 | 1.1            | 0.8                  | 16.5                   |

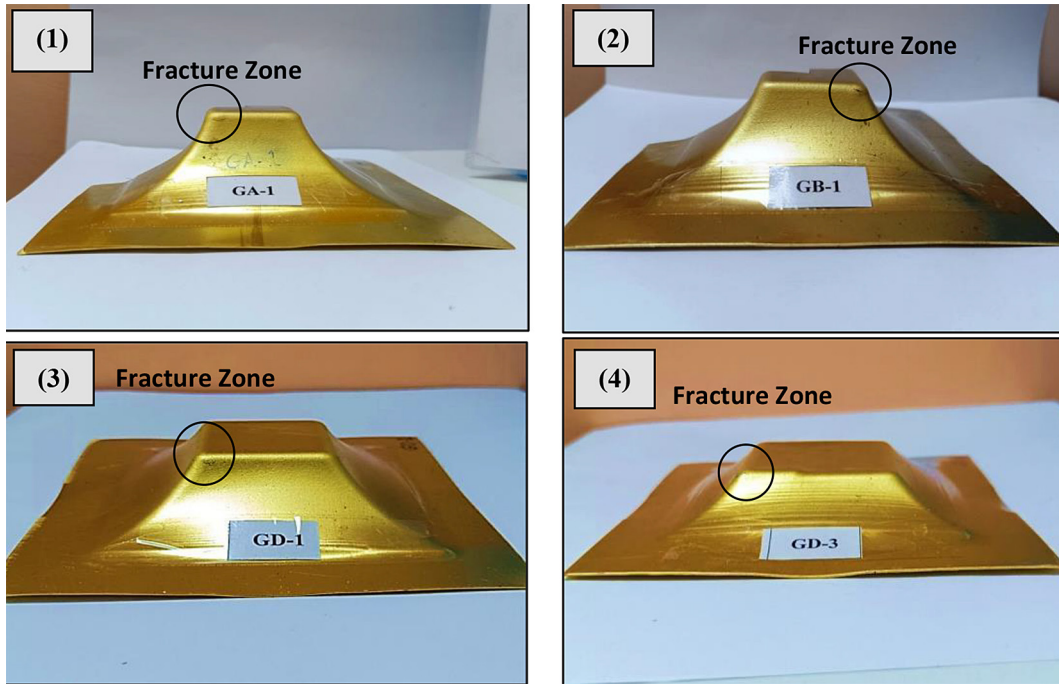


Figure 5. SPIF specimens (Hyperbolic truncated pyramid with varying wall angle)

and the third type is the (Velocity/Angular velocity) type which used to insert the tool rotational speed to the forming tool. Explicit element type has been used to mesh the blank sheet with a sizing of 0.5 mm and through three layers along the edges. This study employs the HDD model to capture fracture during single point incremental forming experiments. The model predicts fracture initiation through voids' nucleation, growth, and coalescence. In this approach, the fracture strain depends solely on stress triaxiality. The Hooputra ductile damage model is represented by the following Equation [20]:

$$\epsilon_{eq}(\eta) = a e^{-c\eta} + b e^{c\eta} \quad (5)$$

Here,  $\epsilon_{eq}$  represents the equivalent plastic strain at fracture;  $\eta = \sigma_H/\sigma_e$  denotes stress triaxiality, where  $\sigma_H$  is the hydrostatic stress and  $\sigma_e$  is the Von Mises equivalent stress; a, b, and c are material parameters determined through testing. Crack initiation occurs in the finite element model when the following condition is met:

$$D = \int_0^{\epsilon_{eq}} \frac{d\epsilon_{eq}}{\epsilon_{eq}(\eta)} = 1 \quad (6)$$

In this context,  $D$  represents the damage variable, which ranges from 0 (virgin material) to 1 (fractured material). Crack initiation and propagation are simulated through element deletion, where an element is removed from the FE model once the damage variable reaches 1.

In order to simulate the SPIF process to investigate the formability of Brass CuZn37, the Excel sheet of time and amplitudes should be prepared to feed the forming tool with motion in three directions (X, Y, Z). This sheet has been prepared by converting the G-codes to amplitudes and time. G-codes have been extracted from the tool path previously generated by the HSMWORKs software. In order to define the materials that will be used in the simulation in ABAQUS software, many mechanical properties (Elastic and Plastic) should be determined for this material; these properties involve density, modulus of elasticity and Poisson's ratio (for the elastic region) which previously illustrated in Table 1, yield stress and plastic strain (for the plastic region) from converting the displacements to strains and loads to stresses after the elastic deformation of the material. These properties have been taken from the tensile testing that was previously conducted in this work.

## RESULTS AND DISCUSSION

### Calculation of HDD parameters

In order to implement the HDD model to investigate the formability of brass CuZn37, two parameters must be calculated: fracture strain and stress triaxiality. These parameters have been

calculated from the tensile test for three different tensile specimens: the first one is the standard specimen (smooth); the second one is the specimen with a notch radius of 4.41 mm, and the third one is the specimen with a notch radius of 1 mm, as depicted in Figure 6. Figure 7 depicts these tensile specimens cut from the brass CuZn37 sheets at 90° (perpendicular) to the rolling direction using a water jet machine. Tensile tests for these specimens have been conducted by a “computer - controlled electronic universal testing machine” in the material engineering department of the University of Technology in order to calculate the fracture strain parameter. This strain value represents the total elongation or deformation the material experienced before breaking. Figure 8 depicts these specimens after the tensile test. The fracture strain parameter for each specimen has been extracted directly from the tensile test results; it is

calculated by taking the strain corresponding to the fracture strength, where the fracture strength is the stress at which the material breaks during a tensile test. To identify it, the tensile test must be performed, then the load-displacement data must be recorded and converted to stress-strain, and the stress at the point of fracture (the last point before the material fails) must be found. The results of the calculated fracture strain have been illustrated in Table 3. The stress triaxiality parameter is calculated by simulating the three different tensile specimens using ABAQUS software. The values of stress triaxiality have been directly exported from ABAQUS to Excel in the form of a Table, and the average values of each specimen have been taken to get the final value of the stress triaxiality for each of these different tensile specimens. The results of the tensile test simulation are

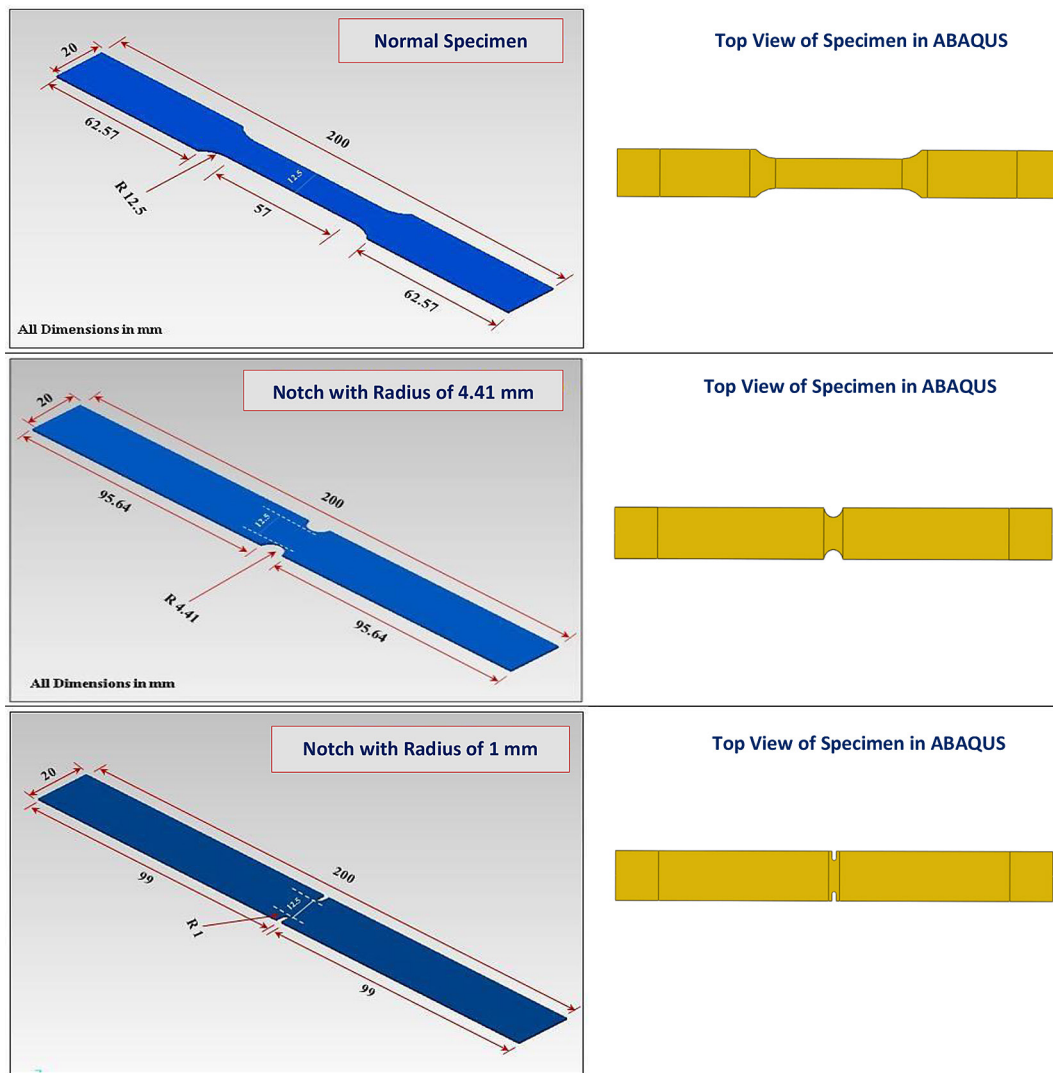
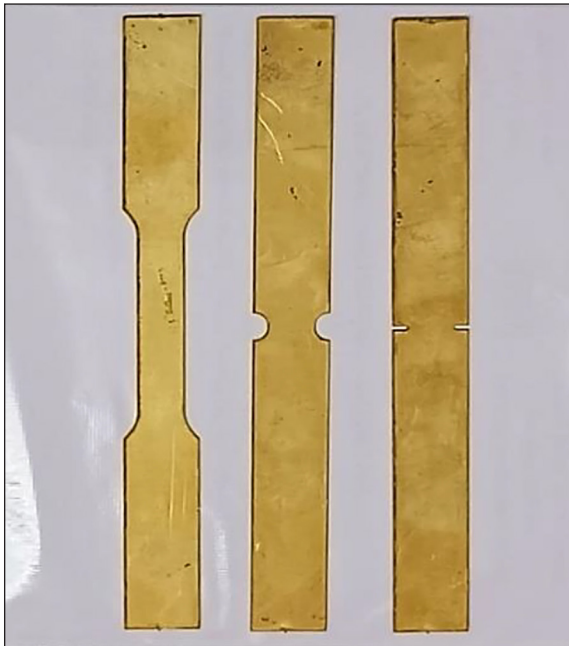


Figure 6. Different design of tensile test specimens



**Figure 7.** The prepared tensile specimens to calculate the HDD model parameters

shown in Figure 9, and Table 4 illustrates the average stress triaxiality of each specimen.

The previous results in Table 4 indicate that when the radius of the notch increases, the stress triaxiality decreases. In order to find an optimal match between the hooputra ductile damage equation (Equation 1) and the measured values of fracture strain and stress triaxiality, a curve fitting procedure was performed in Excel using solver, and the values of hooputra ductile damage parameters (a, b, and c) have been calculated as illustrated in Table 5. Figure 10 depicts the HDD curve, and Table 6 illustrates the set of fracture strain and stress triaxiality values used in the SPIF process simulation. These results indicate that as fracture strain decreases, stress triaxiality increases, and vice versa.

### Verification of hooputra ductile damage model

In this section, the four experiments of SPIF which previously conducted, as illustrated in Table 2 and Figure 5, have been simulated by the Hooputra ductile damage model as a fracture



**Figure 8.** Tensile specimens after performing the tensile test

criterion model by using explicit/abaqus to verify the effectiveness of this model to capture the fracture in SPIF process. Figure 11 depicts the results of this simulation, while Table 7 illustrates the difference between the actual value (the experimental results) and the simulated value of the fracture depth by the Hooputra ductile damage model. The results showed an excellent agreement between the experimental results and the Hooputra ductile damage results, with a total error ratio of 1.91 %, and an agreement ratio of 98.09%.

### Sheet thickness effect on the formability

In this section, a case study using the verified Hooputra ductile damage model has been conducted. This case study includes the impact of the sheet thickness on the formability, specifically in terms of fracture depth of brass CuZn37 formed by a SPIF process. From Table 2, experiment no. 4 has been selected with its constant input parameters as: feed rate of 1200 mm/min, tool rotation speed of 1500 rpm, tool diameter of 10 mm, step size of 1.1 mm and with varying sheet thickness from 0.4 mm to 1.4 mm, so that, six experiments have been performed and as illustrated in Table 8. The results of this case study are depicted in Figure 12. At sheet thicknesses of (0.4, 0.6, 0.8, 1, 1.2, and 1.4) mm, the fracture depth is (14.73, 14.97, 15.30, 15.35, 17.27 and 17.46) mm, respectively.

**Table 3.** Fracture strain values of the different tensile specimens

| CuZn37 | Specimen type   | Normal specimen | Notch of 4.41 mm | Notch of 1 mm |
|--------|-----------------|-----------------|------------------|---------------|
|        | Fracture strain |                 | 0.64856          | 0.14529       |

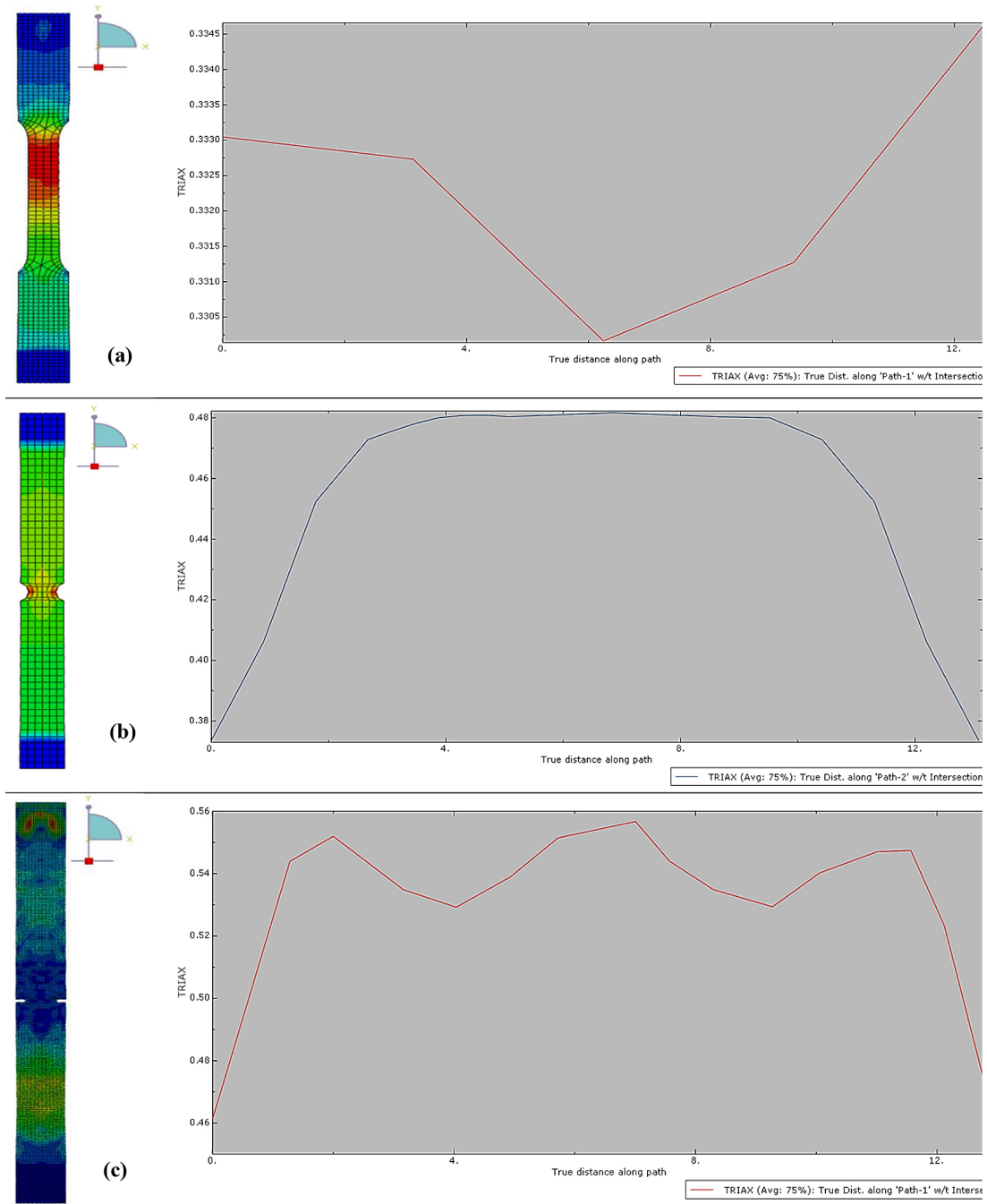


**Figure 9.** Simulation results of stress Triaxiality of (a) normal tensile specimen (b) specimen with notch of 4.41 mm (c) specimen-with notch of 1 mm

**Table 4.** Average stress triaxiality of tensile specimens

| CuZn37 | TRIAX of normal specimen | TRIAX of 4.41 mm notch radius | TRIAX of 1 mm notch radius |
|--------|--------------------------|-------------------------------|----------------------------|
|        | 0.33                     | 0.45                          | 0.53                       |

**Table 5.** HDD parameters

| Parameter | Value     |
|-----------|-----------|
| a         | 48.388    |
| b         | 2.990E-05 |
| c         | 13.078    |

The investigation into the impact of sheet thickness on formability in SPIF processes utilizing the Hooputra ductile damage model in ABAQUS has shown insightful results regarding fracture depth variation. The analysis reveals an

**Table 6.** Values set of fracture strain and stress triaxiality

| No. | Stress triaxiality | Fracture strain |
|-----|--------------------|-----------------|
| 1   | 0.3                | 0.958           |
| 2   | 0.31               | 0.841           |
| 3   | 0.32               | 0.738           |
| 4   | 0.33               | 0.648           |
| 5   | 0.34               | 0.569           |
| 6   | 0.35               | 0.500           |
| 7   | 0.36               | 0.439           |
| 8   | 0.37               | 0.386           |
| 9   | 0.38               | 0.340           |
| 10  | 0.39               | 0.299           |
| 11  | 0.4                | 0.264           |
| 12  | 0.41               | 0.233           |
| 13  | 0.42               | 0.206           |
| 14  | 0.43               | 0.183           |
| 15  | 0.44               | 0.162           |
| 16  | 0.45               | 0.145           |
| 17  | 0.46               | 0.130           |
| 18  | 0.47               | 0.117           |
| 19  | 0.48               | 0.106           |
| 20  | 0.49               | 0.097           |
| 21  | 0.5                | 0.090           |
| 22  | 0.51               | 0.084           |
| 23  | 0.52               | 0.080           |
| 24  | 0.53               | 0.077           |

intriguing relationship between sheet thickness and fracture depth, shedding light on critical aspects of material behavior during the forming process. The results demonstrate a notable trend where fracture depth increases with increasing sheet thickness. This observation aligns with expectations, indicating that thicker sheets can sustain higher levels of deformation before experiencing fracture.

**Sheet thickness effect on the other outputs**

In addition to the influence of the sheet thickness variation on the fracture depth in the SPIF process, it also affects the other output responses. As previously mentioned in this work, six different sheet thicknesses have been used, ranging between (0.4–1.4 mm) to examine the effect of sheet thickness on three other output responses: Von Mises stress (S), equivalent plastic strain (PEEQ), and contact pressure (CPRESS) between the sheet and the forming tool. The results of this section were taken from the simulation work in the previous section as depicted through Figures (13 – 18). Table 9 shows the results of this effect using the hooputra ductile damage model, and Figure 19 depicts the relationship between sheet thickness and the output responses.

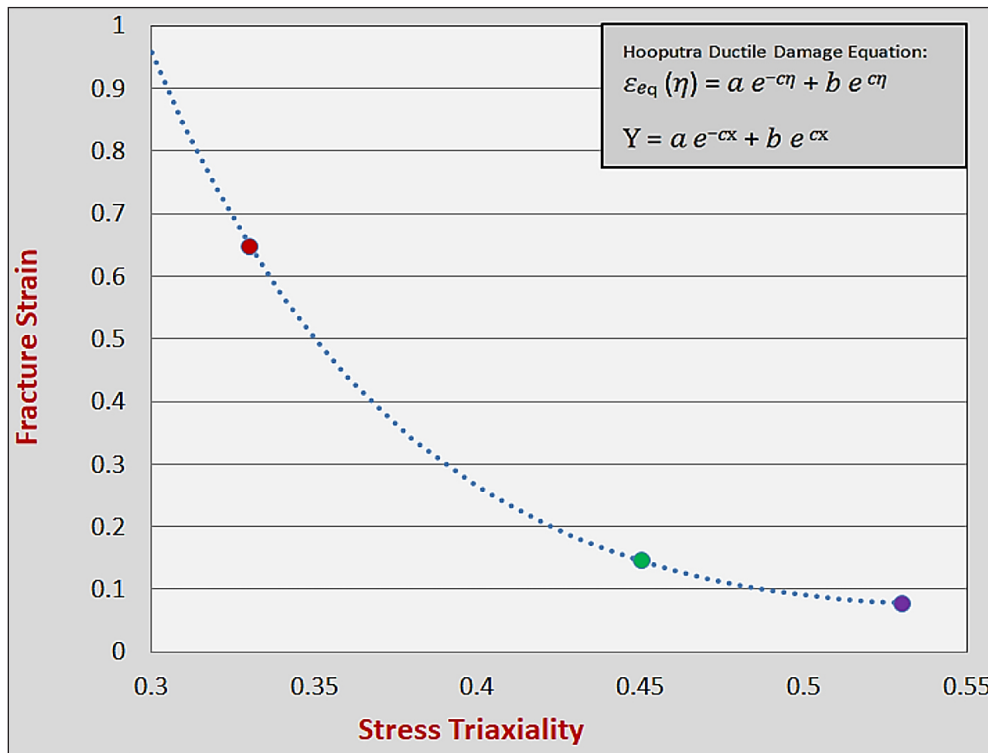


**Figure 10.** Hooputra ductile damage curve

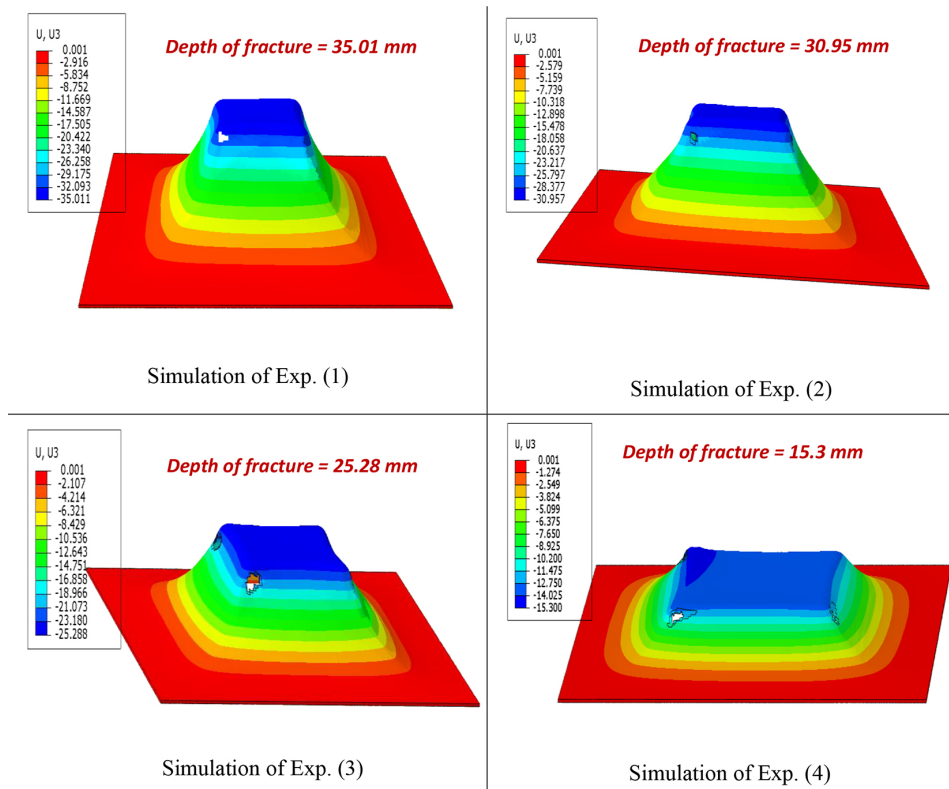


Figure 11. The simulated result of experiments in Table 2 and Figure 4

Table 7. The error value between the actual and simulated values of the fracture depth

| Exp. No. | Actual value (mm) | Simulated value (mm) | Error (mm) |
|----------|-------------------|----------------------|------------|
| 1        | 34.4              | 35.01                | 0.61       |
| 2        | 30.8              | 30.95                | 0.15       |
| 3        | 25.2              | 25.28                | 0.08       |
| 4        | 16.5              | 15.3                 | 1.2        |

Table 8. Input parameters and the output results to predict the effect of sheet thickness on formability

| Exp. No. | Input parameters |                    |                           |                    |                |                      | Simulation output   |
|----------|------------------|--------------------|---------------------------|--------------------|----------------|----------------------|---------------------|
|          | Type of material | Feed rate (mm/min) | Tool rotation speed (rpm) | Tool diameter (mm) | Step size (mm) | Sheet thickness (mm) | Fracture depth (mm) |
| 1        | CuZn37           | 1200               | 1500                      | 10                 | 1.1            | 0.4                  | 14.73               |
| 2        | CuZn37           | 1200               | 1500                      | 10                 | 1.1            | 0.6                  | 14.97               |
| 3        | CuZn37           | 1200               | 1500                      | 10                 | 1.1            | 0.8                  | 15.30               |
| 4        | CuZn37           | 1200               | 1500                      | 10                 | 1.1            | 1                    | 15.35               |
| 5        | CuZn37           | 1200               | 1500                      | 10                 | 1.1            | 1.2                  | 17.27               |
| 6        | CuZn37           | 1200               | 1500                      | 10                 | 1.1            | 1.4                  | 17.46               |

From the results of Table 9 and Figure 19, it is observed that the Von Mises stress slightly increases as the sheet thickness increases. This result is because the shear stresses increase with increasing the sheet thickness, lead to an increase in the Von Mises stress. The relationship between sheet thickness and equivalent

plastic strain is largely influenced by the material’s capacity for plastic deformation and the way stresses are distributed during the forming process. Generally, thinner sheets (0.4 mm) tend to exhibit higher plastic strains since they are easier to deform. In contrast, thicker sheets (0.6–0.8 mm) may initially show lower plastic strain

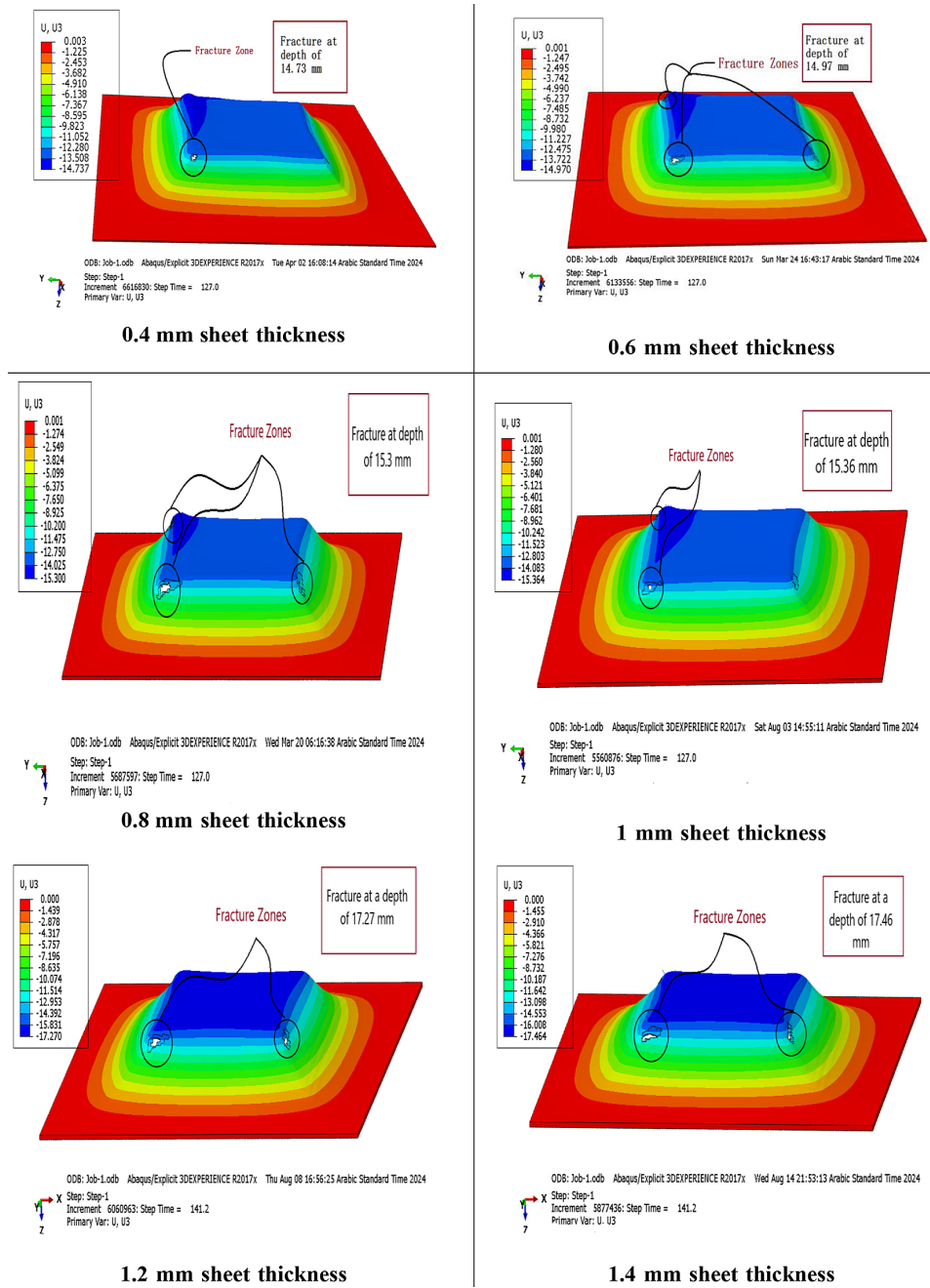


Figure 12. The simulated result of experiments with different sheet thickness

because they resist deformation more. However, the strain can rise again as the thickness increases (1–1.4 mm) due to the greater forming forces needed. The equivalent plastic strain values for the 0.8 mm and 1 mm thick sheets are slightly lower than those observed for the thinnest sheet (0.4 mm). This may be attributed to a balance between the material’s resistance to deformation and the forces applied during forming. At 1.2 mm and 1.4 mm, the rise in equivalent plastic strain indicates that the material experiences more significant plastic deformation as forming

forces increase with thickness. The results also indicated that the relationship between sheet thickness and contact pressure in SPIF generally follows a pattern where contact pressure rises as the sheet thickness increases. This is because thicker sheets typically need more force to deform, resulting in higher contact pressures at the tool-sheet interface.

In summary, the results demonstrate that the relationship between fracture depth and the three output responses is consistent: as the equivalent plastic strain increases, so does the fracture

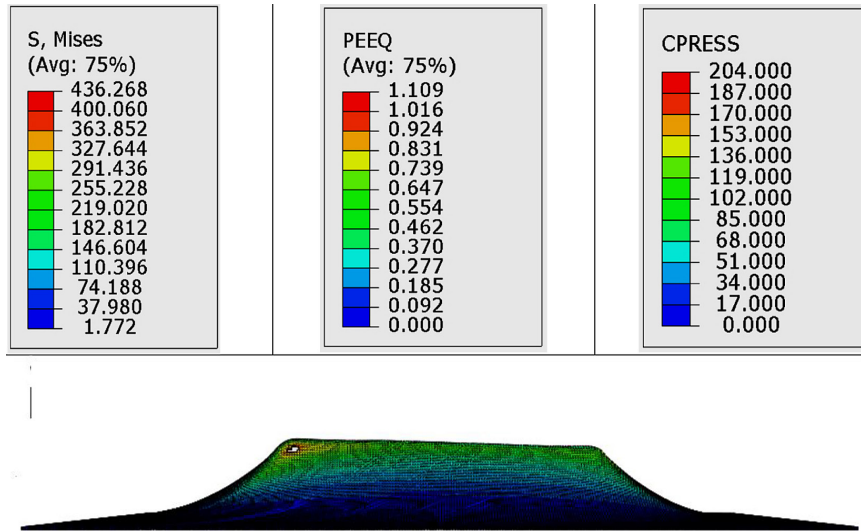


Figure 13. Simulations result of Von Mises stress, equivalent plastic strain, and contact pressure at 0.4 mm sheet thickness

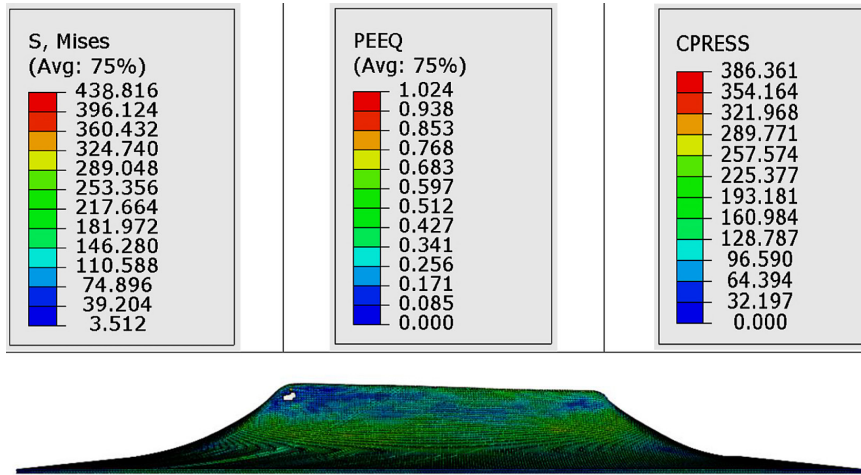


Figure 14. Simulations result of Von Mises stress, equivalent plastic strain, and contact pressure at 0.6 mm sheet thickness

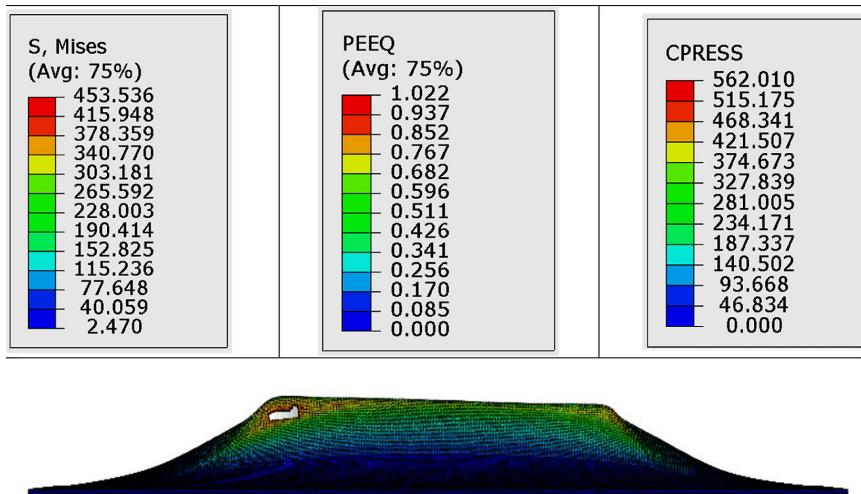


Figure 15. Simulations result of Von Mises stress, equivalent plastic strain, and contact pressure at 0.8 mm sheet thickness

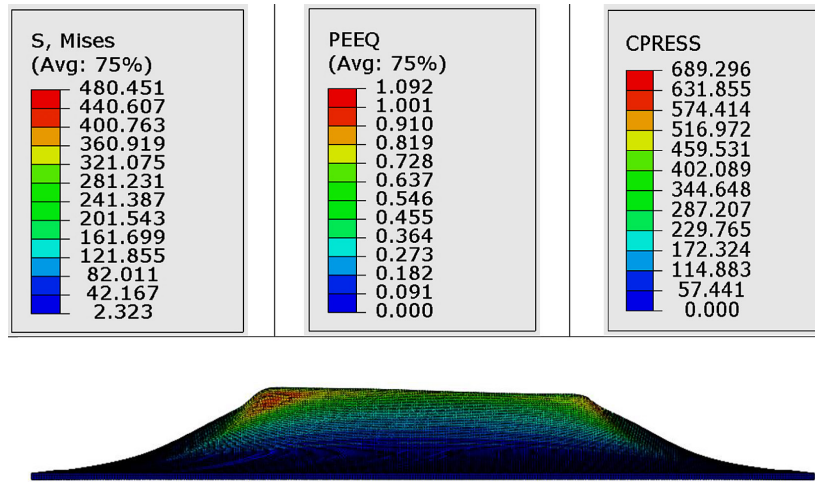


Figure 16. Simulations result of Von Mises stress, equivalent plastic strain, and contact pressure at 1 mm sheet thickness

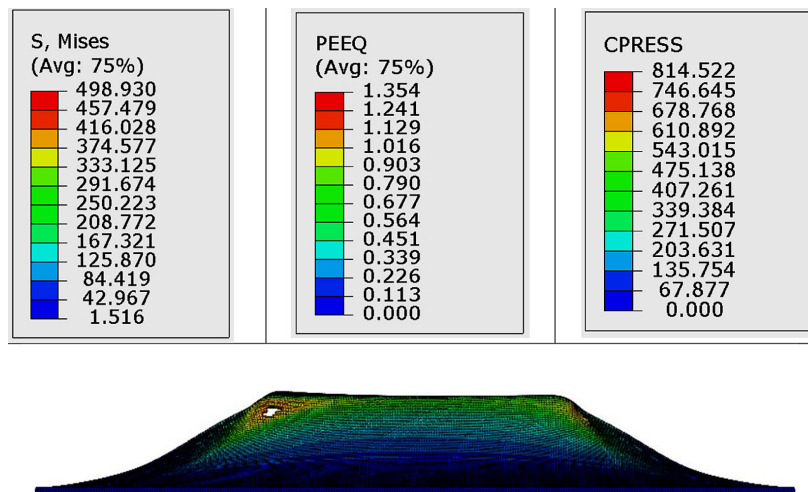


Figure 17. Simulations result of Von Mises stress, equivalent plastic strain, and contact pressure at 1.2 mm sheet thickness

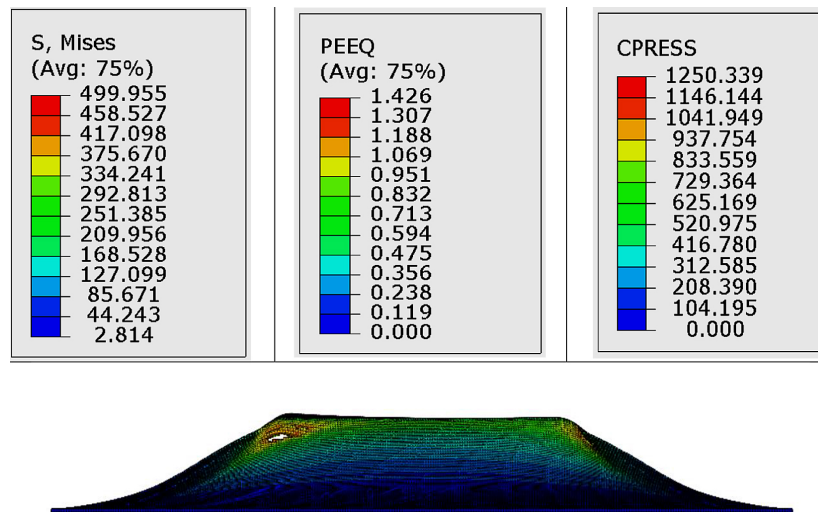
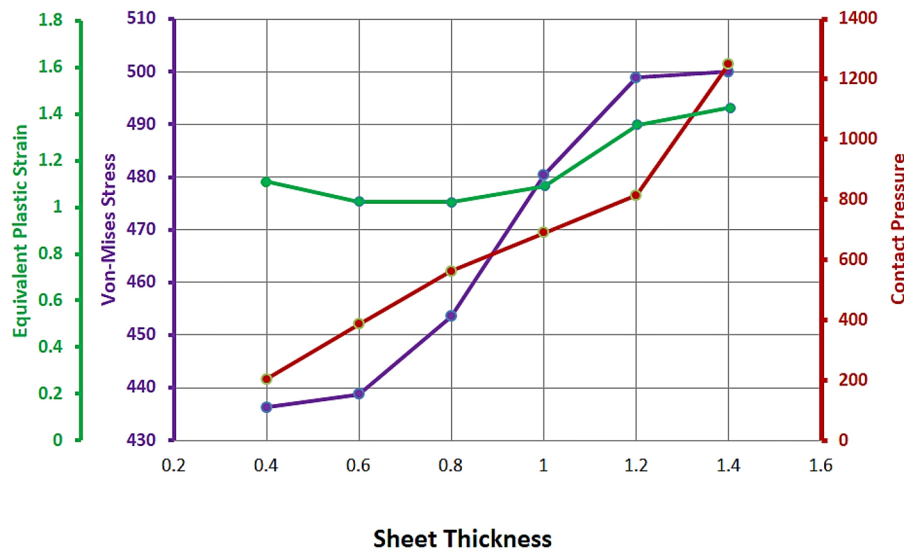


Figure 18. Simulations result of Von Mises stress, equivalent plastic strain, and contact pressure at 1.4 mm sheet thickness

**Table 9.** Effect of sheet thickness on the output responses in SPIF process

| Exp. | Sheet thickness (mm) | Fracture depth (mm) | Von-mises stress (S) (MPa) | Equivalent plastic strain (PEEQ) (mm/mm) | Contact pressure (CPRESS) (MPa) |
|------|----------------------|---------------------|----------------------------|--|---------------------------------|
| 1    | 0.4                  | 14.73               | 436.26                     | 1.109                                    | 204                             |
| 2    | 0.6                  | 14.97               | 438.81                     | 1.024                                    | 386.36                          |
| 3    | 0.8                  | 15.30               | 453.53                     | 1.022                                    | 562                             |
| 4    | 1                    | 15.36               | 480.45                     | 1.092                                    | 689.29                          |
| 5    | 1.2                  | 17.27               | 498.93                     | 1.354                                    | 814.52                          |
| 6    | 1.4                  | 17.46               | 499.95                     | 1.426                                    | 1250.33                         |



**Figure 19.** Relationship between sheet thickness and the output responses in SPIF

depth, which is expected since more significant plastic deformation usually means higher formability before failure. Additionally, higher contact pressures are observed with thicker sheets and greater fracture depths, which is logical because thicker sheets require more force and can endure more deformation before failing. Meanwhile, Von Mises stress increases with thickness and fracture depth, which is reasonable as higher stresses often correlate with more significant deformation before fracture.

## CONCLUSIONS

In this work, the Hooputra ductile damage model in ABAQUS was used to simulate the fracture in the SPIF process of brass CuZn37. Then, a case study has been performed to predict the sheet thickness effect on the formability and the other outputs of the process, and it has concluded the following essential points:

1. The Hooputra ductile damage model precisely captured the ductile fracture behavior of brass CuZn37 in the SPIF process, with a total error ratio and agreement ratio between the actual and simulated results of approximately 1.91% and 98.09%, respectively.
2. The difference in the sheet thickness of brass CuZn37 affects its formability; as the sheet thickness increases from 0.4 mm to 1.4 mm, the formability of brass CuZn37 in terms of fracture depth increases.
3. To obtain a specified product, the Von Mises stress slightly increases with increasing sheet thickness due to the need for greater forming forces for thicker sheets. Consequently, the equivalent plastic strain decreases with increasing sheet thickness from 0.4 mm to 0.8 mm and then increases with increasing sheet thickness from 1 mm to 1.4 mm.
4. The contact pressure increases as the sheet thickness increases, which is acceptable and

consistent with the expected behavior in SPIF. This trend aligns with the process's physical principles, where thicker sheets necessitate greater force, leading to higher contact pressures.

5. Despite this study providing significant insights and results related to the work objectives, the brass CuZn37 used in this work was in the as-delivery condition, meaning that differences in the mechanical properties, microstructure, and surface quality between batches or suppliers were not taken into account. This may affect the generalizability of the results in industrial applications where material conditions can vary.

### Acknowledgements

The authors would like to thank Dr. Shakir Gatea from the University of Nottingham for his scientific support for this work.

### REFERENCES

1. Grimm T.J., Colombini F., and Ragai I. Numerical investigation of step size effect on formability of 2024-T3 aluminum in incremental forming. *J. Manuf. Mater. Process* 2023; 7(70). <https://doi.org/10.3390/jmmp7020070>
2. Habeeb H.A., Jweeg M.J., and Khleif A.A. Effect of the single-point incremental forming process parameters on the surface roughness of aluminum alloy Al 2024-O draw pieces. *Advances in Science and Technology Research Journal* 2023; 17(6): 155–163. <https://doi.org/10.12913/22998624/174364>
3. Ghazi S.K., Bedana A.S., and Salloomb Y. Investigating the impact of process parameters on thinning and formability in aluminum alloy AA 1050 incremental sheet metal forming. *Engineering and Technology Journal* 2023; 41(12): 1653–1659. <https://doi.org/10.30684/etj.2023.143119.1561>
4. Krasowski B., Kubit A., Trzepieciński T., Dudek K., Slota J., Application of X-ray diffraction for residual stress analysis in truncated cones made by incremental forming. *Advances in Science and Technology Research Journal* 2020; 14(2): 103–111. <https://doi.org/10.12913/22998624/118829>
5. Gatea S., Ou H., and McCartney G.. Review on the influence of process parameters in incremental sheet forming. *Int. J. Adv. Manuf. Techn.* 2016; 87(1–4): 479–499. <https://doi.org/10.1007/s00170-016-8426-6>
6. Barrak O.S., Saad M.L., Mezher M.T., Hussein S.K., and Hamzah M.M.. Joining of double pre-holed aluminum alloy AA6061-T6 to polyamide PA using hot press technique. In: *IOP Conference Series: Materials Science and Engineering* 2020; 881(1). <https://doi.org/10.1088/1757-899X/881/1/012062>
7. Ji Y.H. and Park J.J. Incremental forming of free surface with magnesium alloy AZ31 sheet at warm temperatures. *Transactions of Nonferrous Metals Society of China* 2008; 18: 165–169. [https://doi.org/10.1016/S1003-6326\(10\)60195-1](https://doi.org/10.1016/S1003-6326(10)60195-1)
8. Oleksik V., Pascu A., Deac C., Fleacă R., Bologa O. and Racz G.. Experimental study on the surface quality of the medical implants obtained by single point incremental forming. *Int. J. Mater. Form* 2010; 3(1): 935–938. <https://doi.org/10.1007/s12289-010-0922-x>
9. Habeeb H.A., Jweeg M.J., Khleif A.A. Investigation of the Effect of SPIF Parameters on the Thickness of Al 2024 Alloy. *Engineering and Technology Journal* 2023; 41(12): 1627–1637. <https://doi.org/10.30684/etj.2023.143718.1604>
10. Haji Aboutalebi H., and Banhashemi A. Numerical estimation and practical validation of Hooputra's ductile damage parameters. *Int. J. Adv. Manuf. Techn.* 2014; 75: 1701–1710. <https://doi.org/10.1007/s00170-014-6275-8>
11. Kolmogorov W.L. Spannungen Deformationen Bruch. *Metallurgija*.1970; 230–235.
12. Gatea S., Ou H., Lu B., and McCartney G. Modelling of ductile fracture in single point incremental forming using a modified GTN model. *Engineering Fracture Mechanics*, 2017; 186: 59–79. <https://doi.org/10.1016/j.engfracmech.2017.09.021>
13. Shoib Khan and Sharad Pradhan. Experimentation and FE simulation of single point incremental forming. *Materials Today Proceedings* 2019; 27(4). <https://doi.org/10.1016/j.matpr.2019.09.123>
14. Sureshkumar D., and Ethiraj N.. Experimental and finite element analysis of single stage single point incremental forming. *International Journal of Engineering* 2021; 34(10): 2259–2265. <https://doi.org/10.5829/ije.2021.34.10a.07>
15. More S., Kumar A., and Narasimhan K. Parameter identification of GTN damage model using response surface methodology for single point incremental sheet forming of IF steel. *Advances in Materials and Processing Technologies* 2021; 8(2): 1753–1768. <https://doi.org/10.1080/2374068X.2021.1874770>
16. Campanella D., Buffa G., Lo Valvo E., and Fratini L. A numerical approach for the modelling of forming limits in hot incremental forming of AZ31 magnesium alloy. *The International Journal of Advanced Manufacturing Technology* 2021; 114: 3229–3239. <https://doi.org/10.1007/s00170-021-07059-6>
17. Zhang K., Yue Z.M., Su C.J., Wang R., and

- Badreddine H. Modelling of ductile damage in single point incremental forming process using enhanced CDM model. IOP Conf. Series: Materials Science and Engineering, the 19th International Conference on Metal Forming 2022; 1270. <https://doi.org/10.1088/1757-899X/1270/1/012022>
18. Annual Book of ASTM Standards, Library of Congress Catalog Card Number: 83-641658, Printed in Baltimore, MD, USA, 2010.
19. Jagota V., Sethi A.P.S., and Kumar K.. Finite element method: An overview. *Walailak Journal of Science and Technology (WJST)* 2013; 10(1): 1–8. <https://doi.org/10.2004/wjst.v10i1.499>
20. Gatea S. and Ou H.. Experimental testing and numerical modelling of ductile fracture of PEEK in incremental sheet forming process. *Material Research Proceedings* 2024; 41: 1596–1605. <https://doi.org/10.21741/9781644903131-177>